Tracking origins of below-threshold harmonics with a trajectory-resolved fully quantum approach

Rui-Hua Xu,[1,2] Yan-Jun Chen,[3,*] Jie Liu,[1,4] and Li-Bin Fu[1,4,†]
[1]*National Laboratory of Science and Technology on Computational Physics, Institute of Applied Physics and Computational Mathematics, Beijing 100088, China*
[2]*Graduate School, China Academy of Engineering Physics, Beijing 100088, China*
[3]*College of Physics and Information Technology, Shaan'xi Normal University, Xi'an, China*
[4]*HEDPS, Center for Applied Physics and Technology, Peking University, Beijing 100084, China*
(Received 9 June 2016; published 22 December 2016)

The emission of below-threshold harmonics (BTHs) is a promising tool for producing vacuum-ultraviolet frequency combs. Nevertheless, the generation mechanism of BTHs is still an open question and a lot of efforts have been devoted to this issue. Here, with a developed trajectory-resolved fully quantum numerical scheme which allows us to "coherently" trace the motion of the rescattering electron, the complex roles of different rescattering trajectories, such as the first return or multiple returns in the origin of BTHs are identified unambiguously. We show that the emission of BTHs is influenced dramatically by laser intensity. At strong laser fields, multiple returns (especially the third return) play an important role in BTHs. At weak fields, effects related to multiphoton processes dominate. The interference of the different contributions to BTHs is also addressed.

DOI: 10.1103/PhysRevA.94.063417

I. INTRODUCTION

High harmonic generation (HHG) has attracted great interest in the past two decades [1–10]. Previous studies on HHG are mainly focused on higher-order harmonics (HOHs) with energy above the ionization potential I_p of the target. The HOHs can be well described by a semiclassical three-step model [11]. According to this model, the HHG process occurs as a tunnel-ionized continuum electron is driven back into the core by the intense laser field. The movement of the continuum electron can be characterized using rescattering trajectories.

Recently, there has been an increasing interest in studying below-threshold harmonics (BTHs), i.e., harmonics with energy lower than I_p. The BTHs have potential applications as the vacuum-ultraviolet (VUV) light source. Unlike HOHs, the generation of BTHs is very complex. Although the origin of BTHs is usually expected to go beyond the description of the three-step model, there are emerging evidences that rescattering trajectories relating to this model also contribute to BTHs. Yost *et al.* [12] and Power *et al.* [13] showed that the generation of BTHs is influenced importantly by the long trajectory. Soifer *et al.* [14] and Hostetter *et al.* [15] showed that long and short trajectories contribute differently to BTHs, which can be described by a modified three-step model including the Coulomb and the excitation effects. Chini *et al.* [16], Xiong *et al.* [17], and Li *et al.* [18] showed that besides tunneling-related rescattering trajectories, the atomic resonance associated with multiphoton processes such as bound-bound transitions also plays an important role in BTHs. Considering these different mechanisms, a quantitative study which can unambiguously identify the contributions of different rescattering trajectories to BTHs is highly desired.

In this paper, with numerical solution of the time-dependent Schrödinger equation (TDSE) for a three-dimensional model He atom, we study the generation mechanism of BTHs at varied laser intensities and wavelengthes. Furthermore, a scheme is developed based on TDSE simulations with the help of a semiclassical model including the atomic potential, which allows us to "pick out" the contributions of desired trajectories (such as the short trajectory, the long one, or multiple returns) to BTHs. At the same time, the contributions of other rescattering trajectories are well excluded. Our simulations show that multiple returns, especially the third return, contribute substantially to BTHs at high laser intensities as the long trajectory plays a trivial role. At low laser intensities, the main contributions to BTHs, however, come from multiphoton-related processes occurring near the core. The important role of the interference between the different contributions in BTHs is also revealed. Our results have important implications on the origin of BTHs.

The paper is organized as follows. We present our numerical procedure in Sec. II. In Sec. III, we show our main results and analyze the contributions of different rescattering trajectories to BTHs. Section IV is our conclusion.

II. NUMERICAL METHODS

A. Numerical solution of TDSE

The TDSE is solved using the generalized pseudospectral method [19]. We assume that the laser field $\varepsilon(t) = f(t)\varepsilon_0 \sin\omega_0 t$ is linearly polarized along the z direction with the amplitude ε_0, the frequency ω_0, and the envelope function $f(t)$. The Hamiltonian of the model atom studied here is $H(t) = H_0 + z\varepsilon(t)$. $H_0 = \mathbf{p}^2/2 + V(\mathbf{r})$ is the field-free Hamiltonian with the soft-Coulomb potential $V(\mathbf{r}) = -\frac{\alpha}{\sqrt{\mathbf{r}^2+0.5}}$. The parameter α is adjusted such that the ground-state energy of the model atom matches the real one (-0.9 a.u.). We use a trapezoidally shaped laser pulse with a total duration of ten optical cycles and linear ramps of three optical cycles. After each time step the TDSE wave function $\psi(\mathbf{r},t)$ of $H(t)$ with $r \geqslant r_0$ is multiplied by a mask function $M(r) = \cos^{1/4}[\frac{\pi}{2}(r - r_0)/(r_m - r_0)]$ to absorb the continuum wave packet at the boundary. Here, r_0 is the boundary of the

*chenyjhb@gmail.com
†lbfu@iapcm.ac.cn

 ©2016 American Physical Society

absorbing procedure and $r_m = 400$ a.u. is the grid size. The HHG power spectrum $F(\omega)$ for one harmonic ω along the laser polarization $\vec{\mathbf{e}}$ can be evaluated through the Fourier transform of the dipole acceleration [20]. That is,

$$F(\omega) = \left| \int \langle \psi(\mathbf{r},t)|\vec{\mathbf{e}} \cdot \nabla V(\mathbf{r}) + \varepsilon(t)|\psi(\mathbf{r},t)\rangle e^{i\omega t} dt \right|^2. \quad (1)$$

Equation (1) includes the atomic potential $V(\mathbf{r})$ and the laser field $\varepsilon(t)$. Since the laser field is not monochromatic but pulsed, it also contributes to higher harmonics as well. In our cases with the trapezoidally shaped laser pulse, the harmonic orders influenced by the laser field are up to H5. In this paper, we mainly explore the influence of rescattering trajectories on BTHs. In the following discussions, we neglect the influence of this term.

B. Rescattering trajectories for BTHs

Here, we analyze the rescattering trajectories which can contribute to BTHs using a semiclassical electron-ensemble model (SEEM) [21,22]. The SEEM considers the tunneling position and the influence of the Coulomb potential, similar to those used in [14,15]. Figures 1(a) and 1(b) show the evaluated returning energy E_r and the corresponding maximal displacement X_m [23] of the rescattering electron as functions of the return time. The maximal displacement X_m denotes the farthest distance the rescattering electron can arrive at before recombination. Note that the returning energy E_r includes the kinetic energy and the potential energy, and thus it may become negative. We only show the results in which the electrons are released in the second half optical cycle (o.c.) (i.e., 0.5 o.c. $\approx$ 1.0 o.c.).

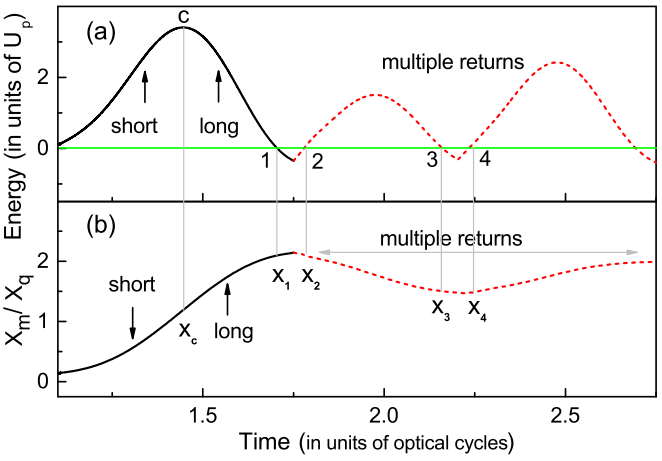

FIG. 1. Returning energy (a) and maximal displacement X_m (b) of the electron as functions of the return time. The black-solid curves show the short and long trajectories. The red-dashed curves indicate multiple returns. The green-horizontal line in (a) shows the zero energy. The long and short trajectories merge together at the cutoff region marked by c. Some typical trajectories which can contribute to BTHs are marked by the numbers 1 (long), 2 and 3 (second return), and 4 (third return). The corresponding maximal displacements X_m of these trajectories are marked by X_c, X_1, X_2, X_3, and X_4, as indicated by the gray vertical lines. The laser intensity is 3×10^{14} W/cm^2 with the wavelength $\lambda = 1200$ nm.

As shown in Fig. 1(a), there are four parts of trajectories (we label them with the number 1–4) which have energy lower than zero; therefore they can contribute to BTHs. These trajectories relate to different return times: trajectory 1 is associated with the long trajectory of the first return; trajectories 2–4 correspond to multiple returns. Comparisons between Figs. 1(a) and 1(b) demonstrate that for different types of trajectories, the maximal displacement X_m is different. By virtue of this observation, we can separate the contributions of desired trajectories from others. For example, (i) with putting the absorbing boundary at $r_0 = X_c = 1.2X_q$ [23] ($X_q = \varepsilon_0/\omega_0^2$ is the quiver amplitude), the possible contributions of all the rescattering trajectories to BTHs are excluded. The harmonic yields (HHG power spectra) obtained with this treatment are denoted using $F_{\text{short}}(\omega)$. We mention that for smaller r_0 such as $r_0 = 8$ a.u., results obtained for BTHs are similar to those with $r_0 = X_c$, implying in this case, the generation process of BTHs occurs near to the core. (ii) Similarly, if we put the boundary at $r_0 = 1.8X_q$, the contributions of trajectories 1 and 2 to BTHs are excluded, but the possible contributions of trajectories 3 and 4 are kept. [Results obtained in this case are not sensitive to the choice of r_0 as $X_3 < r_0 < X_1$, see Fig. 1(b).] We denote the results obtained with $r_0 = 1.8X_q$ using $F_{M+S}(\omega)$. (iii) With increasing the value of r_0, such as $r_0 = 2.5X_q$, we obtain the full TDSE results $F_{\text{full}}(\omega)$, including all of the possible contributions (trajectories 1–4) to HHG. In fact, for $r_0 = 2.1X_q$, just above X_1, results obtained are similar to those with $r_0 = 2.5X_q$.

It should be stressed that the above procedure with $r_0 = 1.8X_q$ for separating the contributions of multiple returns from other rescattering trajectories is applicable only for BTHs. It cannot be applied to the plateau and the cutoff harmonics. For these harmonics, the maximal displacement of the long trajectory coincides with that of multiple returns [see Fig. 1(b)]. As a result, the contributions of multiple returns cannot be separated from the long ones. Instead, with setting $r_0 = X_c$, one can separate the contributions of the short trajectory from others and obtain the short-trajectory results $F_{\text{short}}(\omega)$ for the plateau and the cutoff harmonics [23]. It should also be noted that the short-trajectory results $F_{\text{short}}(\omega)$ for BTHs are different from those for the plateau and the cutoff harmonics. For the BTHs, the results $F_{\text{short}}(\omega)$ imply that the main contributions to harmonic emission come from multiple-photon processes, since the short rescattering trajectory doesn't contribute to BTHs. For the plateau and the cutoff harmonics, the results $F_{\text{short}}(\omega)$ indeed imply that the main contributions to HHG arise from the short rescattering trajectory. The above discussions will help one to understand the following results in Figs. 2–5.

III. RESULTS AND DISCUSSION

A. Roles of multiple returns

Next, we explore the contributions of different rescattering trajectories to BTHs. In Fig. 2 we show the laser-intensity dependence of the ratio $F_{\text{full}}(\omega)/F_{\text{short}}(\omega)$ for several BTHs at different laser wavelengths. It should be noted that due to the destructive interference between the contributions of multiphoton processes and rescattering trajectories, the value of $F_{\text{full}}(\omega)/F_{\text{short}}(\omega)$ may be smaller than unity. As one can

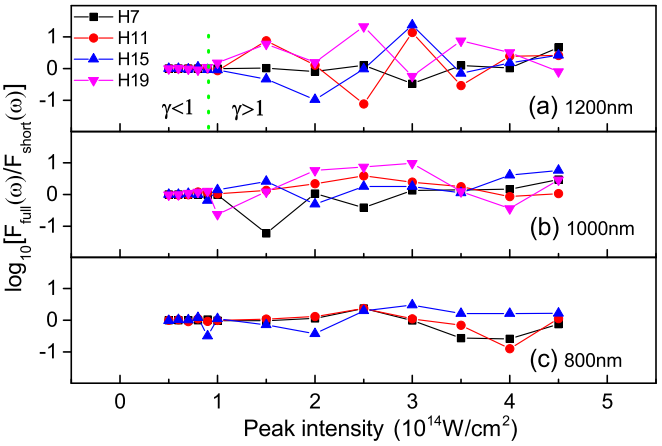

FIG. 2. Ratio of $F_{\text{full}}(\omega)/F_{\text{short}}(\omega)$ as a function of the laser intensity for H7, H11, H15, and H19 at different laser wavelengths: (a) 1200 nm, (b) 1000 nm, and (c) 800 nm.

see, the results at different wavelengths are similar. As an example, we discuss the results of 1200 nm in Fig. 2(a). Clearly, when the laser intensity is lower than $1 \times 10^{14}\text{W/cm}^2$ with the Keldysh parameter $\gamma = \sqrt{I_p/2U_p} \geqslant 1$, the value of $\log_{10}[F_{\text{full}}(\omega)/F_{\text{short}}(\omega)]$ is near to zero, which means that at low laser intensities, rescattering trajectories contribute little to BTHs. With high laser intensities, this value is far away from zero, suggesting the important role of rescattering trajectories in the emission of BTHs, in agreement with previous studies [12,13].

To illuminate this point, in Fig. 3 we show the comparison between the harmonic spectra obtained with different absorbing procedures, i.e., $F_{\text{full}}(\omega)$ (square), $F_{\text{short}}(\omega)$ (circle), and $F_{M+S}(\omega)$ (triangle). As shown in Fig. 3(a), when the laser intensity is low, all of the curves almost coincide with each other for lower harmonic orders, which implies that the BTHs mostly originate from multiphoton processes. However, when the laser intensity increases, the situation is very different.

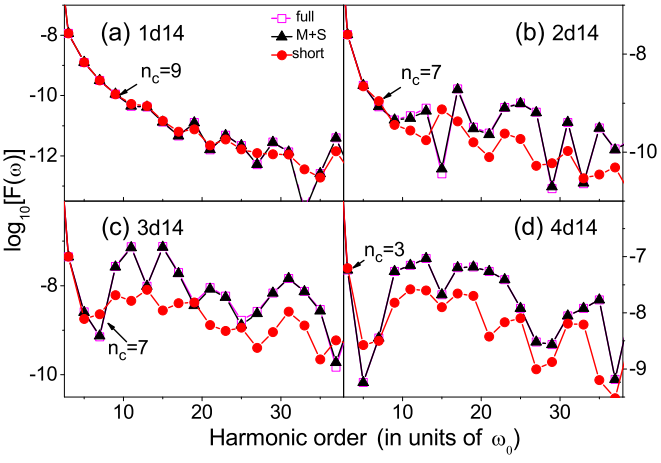

FIG. 3. Harmonic spectra obtained with different absorbing procedures at different laser intensities (W/cm^2): (a) 1×10^{14}, (b) 2×10^{14}, (c) 3×10^{14}, and (d) 4×10^{14}. The laser wavelength is $\lambda = 1200$ nm. n_c denotes the lowest harmonic order that rescattering trajectories can contribute to, as predicted from the SEEM.

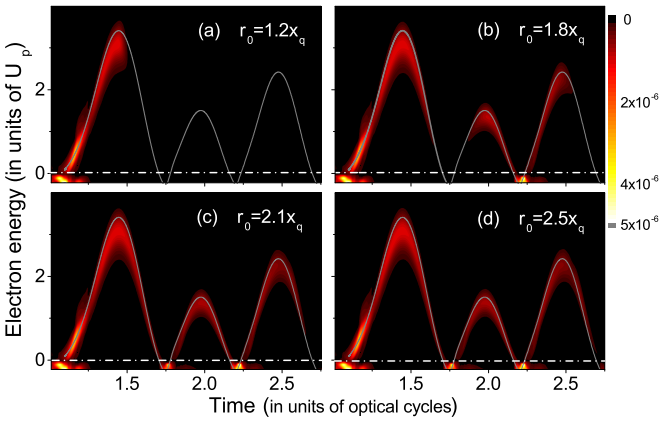

FIG. 4. Rescattering energy and time distributions (the color coding) obtained from TDSE simulations at $I = 3 \times 10^{14}$ W/cm^2 and $\lambda = 1200$ nm with different absorbing boundaries r_0, as shown. In each panel, the SEEM prediction of the rescattering trajectories is also shown (the solid curve).

As presented in Figs. 3(b)–3(d), the curves of F_{full} and F_{M+S} also agree with each other, but they begin to deviate remarkably from the curve of F_{short}. This agreement between the F_{full} and F_{M+S} curves suggests that trajectories 1 and 2 in Fig. 1(a) almost do not contribute to BTHs, since for F_{M+S} the contributions of these two trajectories are excluded. At the same time, this remarkable deviation of the F_{M+S} curve from the F_{short} one (where the contributions of all rescattering trajectories are excluded) implies that trajectories 3 and 4 in Fig. 1(a), relating to multiple returns, greatly affects BTHs. Figures 3(b)–3(d) also show that the lowest order from which this deviation begins is near to n_c of the SEEM prediction, which is lower for higher laser intensities [17].

To further check our results and give an intuitive insight into the generation mechanism of BTHs, the time-energy distribution of the rescattering wave packet for the model atom is plotted in Fig. 4. To obtain these distributions, as in [24], we project the TDSE wave function in the inner region (which is defined as $\psi(\mathbf{r},t)$ with $r \leqslant 10$ a.u.) on the real-basis eigenstates of H_0 in each time step. The TDSE simulations are performed with different absorbing procedures as discussed in Fig. 1. For clarity, only the relevant simulations in which the electrons are emitted in the second half-optical cycle [24] are presented.

For the case of $r_0 = 1.2X_q$ in Fig. 4(a), the distribution shows a clear short-trajectory branch in the energy region of $E_r > 0$ which closely matches the SEEM prediction (the solid curve). The distribution also shows a large amplitude at $E_r < 0$ to which the rescattering trajectories do not contribute. Therefore we expect that this large amplitude at $E_r < 0$ arises from bound-bound transitions or the transitions between the laser dressed states. For $r_0 = 1.8X_q$ in Fig. 4(b), following the solid curve, the distribution shows more branches at $E_r > 0$. In particular, a large amplitude around $t = 2.25T$ with $E_r < 0$ emerges, which also agrees with the SEEM predictions [trajectories 3 and 4 in Fig. 1(a)]. Here, $T = 2\pi/\omega_0$ is the laser cycle. A careful analysis also shows that this large amplitude is mainly associated with the time-frequency region of trajectory 4 here. Results in Figs. 4(c) and 4(d) are similar. Here, a large amplitude appears around $t = 1.75T$ [trajectories

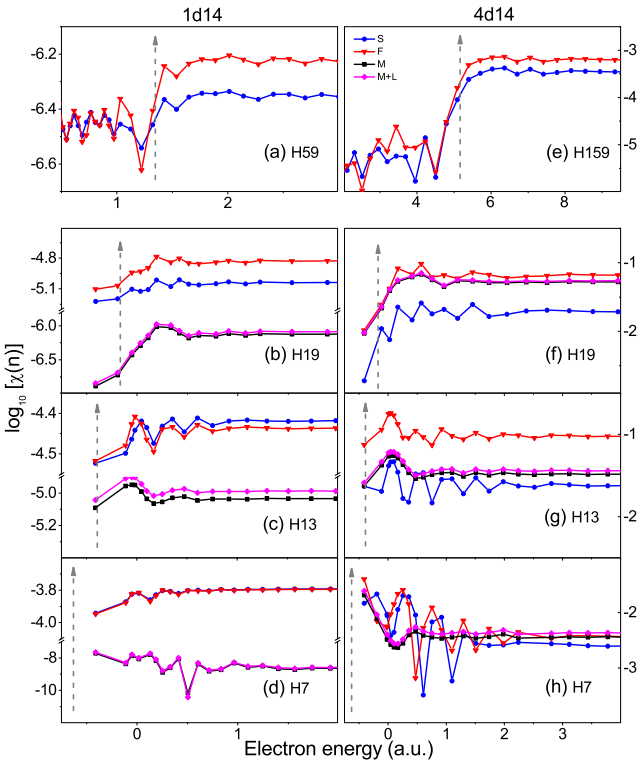

FIG. 5. Contribution of $\chi(n) = |\sum_{n'=0}^{n'=n} G(n',\omega)|^2$ to some harmonics ω as a function of the electron energy E_n (i.e., the energy of the nth eigenstate $|n\rangle$), at $I = 1\times10^{14}\mathrm{W/cm^2}$ (the left column) and $4\times10^{14}\mathrm{W/cm^2}$ (the right column) with $\lambda = 1200$ nm. The harmonics are calculated with different absorbing procedures: (i) The blue-circle curves show the contribution $\chi_S = |\sum_{n'} G_{\mathrm{short}}|^2$ related to $r_0 = 1.2X_q$. (ii) The red-triangle curves show the contribution $\chi_F = |\sum_{n'} G_{\mathrm{full}}|^2$ related to $r_0 = 2.5X_q$. (iii) The contribution related to $r_0 = 1.8X_q$ can be denoted using $|\sum_{n'} G_{S+M}|^2$. Through the expression of $\sum_{n'} G_M = \sum_{n'}(G_{S+M} - G_{\mathrm{short}})$, one can obtain only the contribution $\chi_M = |\sum_{n'} G_M|^2$ of trajectories 3 and 4 in Fig. 1(a), as indicated by the black-square curves. (iv) The magenta-diamond curves are obtained with the relation $\sum_{n'} G_{M+L} = \sum_{n'}(G_{\mathrm{full}} - G_{\mathrm{short}})$ and contain only the contribution $\chi_{M+L} = |\sum_{n'} G_{M+L}|^2$ of trajectories 1–4 in Fig. 1(a). Since the procedure with $r_0 = 1.8X_q$ relating to the contributions χ_M and χ_{M+L} is not applicable for the cutoff harmonics of H59 and H159, in Figs. 5(a) and 5(e) we show only the curves of χ_S and χ_F. For clarity, data points in the continuum region ($E_n > 0$) are shown partly.

1 and 2 in Fig. 1(a)] and is mainly related to the region of trajectory 2. As the amplitude around $t = 2.25T$ is remarkably larger than that around $t = 1.75T$, one can conclude that the main contribution to BTHs comes from the third return (trajectory 4), and the second return (trajectory 2) plays a small role. These results in Fig. 4 imply the applicability of our TDSE absorbing procedure. Particularly, they give direct observations to the important role of multiple returns (instead of the first return of trajectory 1) in BTHs. Multiple returns have shown the importance in nonsequential double ionization and the emission of HOHs, and this importance has been identified as arising from the Coulomb focusing [25,26]. Based on the above results, we predict that the Coulomb focusing also has a strong influence on BTHs. Since rescattering trajectories arise from tunneling ionization of the bound electron and the latter depends on the laser intensity, the contribution of multiple returns to BTHs also does so, as seen in Figs. 2 and 3.

B. Interference of different contributions

To understand the origin of BTHs deeply, we further study the different contributions with a fully quantum analysis. We project the TDSE wave function $\psi(\mathbf{r},t)$, obtained with different absorbing procedures, on the eigenstates of H_0. Then the HHG power spectrum can be approximately evaluated with [27]

$$F(\omega) \approx \left|\sum_n G(n,\omega)\right|^2, \tag{2}$$

where the expression of the function $G(n,\omega)$ is

$$G(n,\omega) = \langle 0|\vec{\mathbf{e}}\cdot\nabla V|n\rangle \int dt a_0^*(t) a_n(t) e^{i\omega t}. \tag{3}$$

Here, $|n\rangle$ with $n = 0,1,2\ldots$ represents the eigenstate of H_0 (including all the bound and continuum states) with energy E_n. $|0\rangle$ is the ground state. $a_n(t) = \langle n|\psi(\mathbf{r},t)\rangle$ is the amplitude. In Eqs. (2) and (3), we consider only the contributions of the excited or ionized electrons which transit back to the ground state $|0\rangle$. This treatment is somewhat similar to the strong-field approximations [2], where the transitions of the continuum electrons $|\mathbf{p}\rangle$ back to only the ground state $|0\rangle$ are considered to contribute most to HHG. The HHG spectra evaluated with Eqs. (2) and (3) are very similar to those obtained with Eq. (1), allowing a fully quantum analysis of HHG as shown in Fig. 5.

Figure 5 plots the integrated contribution

$$\chi(n) = \left|\sum_{n'=0}^{n'=n} G(n',\omega)\right|^2 \tag{4}$$

for harmonics located in different energy regions. The harmonics are evaluated with different absorbing procedures as introduced in Sec. II B. The gray-dashed arrow indicates the energy E_n whose value agrees with the energy conservation relation $\omega = m\omega_0 = E_n + I_p$ [5]. Here, m is the harmonic order and I_p is the ionization potential of the ground state.

First, for comparison, in Figs. 5(a) and 5(e) we plot the results for the cutoff harmonics of H59 and H159 at different laser intensities. For H59 of the low-intensity case in Fig. 5(a), one can observe that the short-trajectory result χ_S (blue circle) is comparable to the full one χ_F (red triangle), implying that the different rescattering trajectories, including long and short trajectories, play a similar role in the emission of this harmonic order. In addition, the results in Fig. 5(a) also show that the main contribution to this order comes from the electron with energy E_n agreeing with the energy conservation relation $\omega = E_n + I_p$. The yield of this order increases remarkably around the dashed arrow. The phenomenon differs remarkably from that for BTHs (see the cases of H7, H13, and H19 in Fig. 5). For H159 of the high-intensity case in Fig. 5(e), the situation is similar.

Second, for H19 near the threshold, the curves of χ_S (blue circle) and χ_F (red triangle) are also comparable to each other, but they are remarkably higher than other curves of χ_M and

χ_{M+L} in Fig. 5(b). Since the rescattering trajectories responsible for BTHs are associated with only the long trajectory and multiple returns and the short rescattering trajectory doesn't contribute to BTHs, the above results imply that the main contributions to H19 come from multiphoton processes such as bound-bound transitions. In addition, because the χ_F curve is somewhat higher than the χ_S curve, one can expect that the interference of different contributions relating to rescattering trajectories and multiphoton processes also plays a role in the emission of this order. For the high-intensity case in Fig. 5(f), one can observe that the χ_F curve almost coincides with the curve of χ_M (black square) and is comparable with that of χ_{M+L} (magenta diamond), suggesting that rescattering trajectories relating to multiple returns contribute mostly to this order.

Third, for H13 below the threshold in Fig. 5(c), the χ_F curve is comparable with that of χ_S (blue circle). Since the latter does not include the contributions of rescattering trajectories, one can conclude that multiphoton processes dominates in this order as for the case of H19 in Fig. 5(b). For the high-intensity case in Fig. 5(g), the curves of χ_M and χ_{M+L} are near to each other and they are comparable with that of χ_S, implying the mixed contributions of multiphoton processes and tunneling-related rescattering trajectories. Since the χ_F curve is remarkably higher than other curves, one can also conclude that the interference of these contributions plays an important role in this order.

Fourth, for the low order H7 in Fig. 5(d), the curves of χ_F and χ_S agree with each other, indicating the dominating role of multiphoton processes in this order. For the high-intensity case in Fig. 5(h), all of the curves are close to each other, showing the comparable contributions of multiphoton processes and tunneling-related rescattering trajectories.

It is worth noting that for the cases of BTHs in Fig. 5, only in Fig. 5(f) do we observe the dominating contribution of the rescattering trajectories. For other cases of BTHs in Fig. 5, the main contributions come from multiphoton processes [as in Figs. 5(b)–5(d)] or a mixed contribution of multiphoton processes and rescattering trajectories which are associated with the tunneling dynamics of the electron [as in Figs. 5(g) and 5(h)]. The results show the complex origins of BTHs, in agreement with our previous analyses. In particular, they disclose the nontrivial role of the interference effect in BTHs. We have checked the main results in this paper for other target atoms such as H and Ar.

Before concluding, we append that in the above discussions on the generation mechanism of BTHs, we mainly consider the effects of the ionized electron rescattering trajectories and do not take into account the atomic structure. To obtain deeper insights into the complex origins of BTHs as revealed in Fig. 5, a full analysis in terms of (i) the excited states of the neutral system and (ii) the excited states of the singly ionized system is needed.

IV. CONCLUSION

In summary, the origin of BTHs has been studied with a trajectory-resolved fully quantum approach based on TDSE simulations. With differentiating the contributions of different rescattering trajectories from each other, the role of multiple returns in BTHs is identified. The generation mechanism of BTHs is shown to depend strongly on the laser intensity. As the contributions related to rescattering trajectories play an important role in the case of high laser intensities, the contributions arising from multiphoton processes prevail in the low-intensity case. The interference between these different contributions is also found to have a nontrivial influence on BTHs. Experimentally, with controlling the electron trajectories [28–30], it is possible to "observe" the interference of these different contributions and modulate the yields of BTHs.

ACKNOWLEDGMENTS

This work is supported by the National Basic Research Program of China (973 Program) (Grant No. 2013CB834100) and the National Natural Science Foundation of China (Grants No. 11374040, No. 11274051, No. 11274090, No. 11475027, and No. 11575027).

[1] A. L'Huillier, K. J. Schafer, and K. C. Kulander, J. Phys. B: At., Mol. Opt. Phys. **24**, 3315 (1991).
[2] M. Lewenstein, Ph. Balcou, M. Yu. Ivanov, A. L'Huillier, and P. B. Corkum, Phys. Rev. A **49**, 2117 (1994).
[3] P. Salieres, B. Carre, L. Le Deroff, F. Grasbon, G. G. Paulus, H. Walther, R. Kopold, W. Becker, D. B. Milosevic, A. Sanpera, and M. Lewenstein, Science **292**, 902 (2001).
[4] M. Hentschel, R. Kienberger, Ch. Spielmann, G. A. Reider, N. Milosevic, T. Bracbec, P. B. Corkum, U. Heinzmann, M. Drescher, and F. Krausz, Nature (London) **414**, 509 (2001).
[5] J. Itatani, J. Levesque, D. Zeidler, Hiromichi Niikura, H. Pepin, J. C. Kieffer, P. B. Corkum, and D. M. Villeneuve, Nature (London) **432**, 867 (2004).
[6] G. Sansone, E. Benedetti, F. Calegari, C. Vozzi, L. Avaldi, R. Flammini, L. Poletto, P. Villoresi, C. Altucci, R. Velotta, S. Stagira, S. De Silvestri, and M. Nisoli, Science **314**, 443 (2006).
[7] T. Morishita, A. T. Le, Z. Chen, and C. D. Lin, Phys. Rev. Lett. **100**, 013903 (2008).
[8] H. J. Wörner, J. B. Bertrand, D. V. Kartashov, P. B. Corkum, and D. M. Villeneuve, Nature (London) **466**, 604 (2010).
[9] T. Popmintchev, M.-C. Chen, D. Popmintchev, P. Arpin, S. Brown, S. Ališauskas, G. Andriukaitis, T. Balčiunas, O. D. Mücke, A. Pugzlys, A. Baltuška, B. Shim, S. E. Schrauth, A. Gaeta, C. Hernández-García, L. Plaja, A. Becker, A. Jaron-Becker, M. M. Murnane, and H. C. Kapteyn, Science **336**, 1287 (2012).
[10] M. Th. Hassan, T. T. Luu, A. Moulet, O. Raskazovskaya, P. Zhokhov, M. Garg, N. Karpowicz, A. M. Zheltikov, V. Pervak, F. Krausz, and E. Goulielmakis, Nature (London) **530**, 66 (2016).

[11] P. B. Corkum, Phys. Rev. Lett. **71**, 1994 (1993).
[12] D. C. Yost, T. R. Schibli, J. Ye, J. L. Tate, J. Hostetter, M. B. Gaarde, and K. J. Schafer, Nat. Phys. **5**, 815 (2009).
[13] E. P. Power, A. M. March, F. Catoire, E. Sistrunk, K. Krushelnick, P. Agostini, and L. F. DiMauro, Nat. Photonics **4**, 352 (2010).
[14] H. Soifer, P. Botheron, D. Shafir, A. Diner, O. Raz, B. D. Bruner, Y. Mairesse, B. Pons, and N. Dudovich, Phys. Rev. Lett. **105**, 143904 (2010).
[15] J. A. Hostetter, J. L. Tate, K. J. Schafer, and M. B. Gaarde, Phys. Rev. A **82**, 023401 (2010).
[16] M. Chini, X. W. Wang, Y. Cheng, H. Wang, Y. Wu, E. Cunningham, P. C. Li, J. Heslar, D. A. Telnov, S. I. Chu, and Z. H. Chang, Nat. Photonics **8**, 437 (2014).
[17] Wei-Hao Xiong, Ji-Wei Geng, Jing-Yi Tang, Liang-You Peng, and Qihuang Gong, Phys. Rev. Lett. **112**, 233001 (2014).
[18] Peng-Cheng Li, Yae-Lin Sheu, Cecil Laughlin, and Shih-I Chu, Nat. Commun. **6**, 7178 (2015).
[19] Xiao-Min Tong and Shih-I Chu, Chem. Phys. **217**, 119 (1997).
[20] M. Lein, N. Hay, R. Velotta, J. P. Marangos, and P. L. Knight, Phys. Rev. Lett. **88**, 183903 (2002).
[21] L. B. Fu, J. Liu, J. Chen, and S. G. Chen, Phys. Rev. A **63**, 043416 (2001).
[22] L. B. Fu, G. G. Xin, D. F. Ye, and J. Liu, Phys. Rev. Lett. **108**, 103601 (2012).
[23] S. Yu, B. Zhang, Y. Li, S. Yang, and Y. Chen, Phys. Rev. A **90**, 053844 (2014).
[24] X. M. Tong, S. Watahiki, K. Hino, and N. Toshima, Phys. Rev. Lett. **99**, 093001 (2007).
[25] G. L. Yudin and M. Y. Ivanov, Phys. Rev. A **63**, 033404 (2001).
[26] J. Tate, T. Auguste, H. G. Muller, P. Saliéres, P. Agostini, and L. F. DiMauro, Phys. Rev. Lett. **98**, 013901 (2007).
[27] Y. J. Chen, J. Liu, and B. Hu, Phys. Rev. A **79**, 033405 (2009).
[28] P. Antoine, A. L'Huillier, and M. Lewenstein, Phys. Rev. Lett. **77**, 1234 (1996).
[29] G. Sansone, E. Benedetti, J.-P. Caumes, S. Stagira, C. Vozzi, S. De Silvestri, and M. Nisoli, Phys. Rev. A **73**, 053408 (2006).
[30] A. Zaïr, M. Holler, A. Guandalini, F. Schapper, J. Biegert, L. Gallmann, U. Keller, A. S. Wyatt, A. Monmayrant, I. A. Walmsley, E. Cormier, T. Auguste, J. P. Caumes, and P. Salières, Phys. Rev. Lett. **100**, 143902 (2008).